Dyes and Pigments 84 (2010) 1–13

Contents lists available at ScienceDirect

Dyes and Pigments

journal homepage: www.elsevier.com/locate/dyepig

The synthesis of novel, unsymmetrically substituted, chiral naphthalene and perylene diimides: Photophysical, electrochemical, chiroptical and intramolecular charge transfer properties

Suleyman Asir [a], Ayhan S. Demir [b], Huriye Icil [a,*]

[a] Department of Chemistry, Faculty of Arts and Science, Eastern Mediterranean University, Famagusta, N.Cyprus Mersin 10, Turkey
[b] Department of Chemistry, Middle East Technical University, 06531 Ankara, Turkey

ARTICLE INFO

Article history:
Received 21 January 2009
Received in revised form
7 April 2009
Accepted 8 April 2009
Available online 20 May 2009

Keywords:
Unsymmetrical naphthalene diimides
Unsymmetrical perylene diimides
Chirality
Charge transfer
Exciplex
Cyclic voltammetry

ABSTRACT

A novel naphthalene monoimide and two unsymmetric chiral diimides (naphthalene and perylene) were synthesized; for comparison purposes, the perylene monoimide with the same substituent in the naphthalene monoimide was prepared. The naphthalene monoimide exhibited intramolecular charge transfer complexation in polar solvents. Excimer-like emissions were obtained in non-polar, polar protic and aprotic solvents in the cases of both the naphthalene monoimide and diimide. The specific optical rotation values of unsymmetrical chiral naphthalene and perylene diimides were −221.6 and −24, respectively at 20 °C. The Chiral naphthalene diimide showed prominent, negative Cotton effects centred at 362 and 382 nm in CH_3CN.

1. Introduction

Although significant advances in the synthesis of chiral naphthalene and perylene diimides have been made, the synthesis of macromolecules with inherently strong chiral properties remains a challenge. The optical property of helically chiral compounds depends strongly on the helical structure (conjugation and dihedral angle). There has been a growing interest in the development of new chiral molecular switches [1–3]. Moreover, the area using molecular chirality to engineer useful properties in nanoscience materials is fruitful and exciting, and represents an exceptionally strong promise for future development. Many types of achiral, perylene and naphthalene diimides have been synthesised and their attractive properties for photonic materials, molecular devices and biological applications have been well reported in literature [4–14]. Chiral perylene and naphthalene diimides are particularly very promising classes of dyes for chiral molecular switches due to their excellent photochemical and electrochemical properties, and good thermal stabilities.

Introduction of chirality into naphthalene and perylene diimides remains a challenge and may lead to materials with optimized optical properties that can emit circularly polarized light. Several helical naphthalene and perylene diimides with strong CD (circular dichroism) effects have been prepared with optimized optical properties [15–24]. Unsymmetric chiral perylene diimides have been synthesized with the same method used for achiral unsymmetric perylene dyes synthesis [25]. By substituent tuning the face-to-face π–π interaction of perylene dyes can be tailored in order to achieve a balance between good solubility and the ability to form stacks with extensive intermolecular π orbital overlap, which is very important for applications envisaged in the area of photonics [19,21]. Importantly, enhancement of structural stability should be taken into account when tailoring the structures in order to provide efficient chiroptical switching. Recently, the first solution-processable nonracemic chiral main-chain perylene polymers have been prepared which emerged as a promising helical polymer for use in optoelectronic devices [23]. NDI (naphthalene diimide) and PDI (perylene diimide) derivatives are able to intercalate inside DNA [26–33]. Additionally, it is possible to increase their binding property via conjugation to other binding species, nucleic acids [28–33]. The facile reduction of these compounds has allowed them to be used as electrochemical DNA biosensors for the detection of specific genes [29]. Naphthalene modified cyclic D, L–peptide nanotubes with interesting optical and electronic properties have been well documented [34,35]. On the other hand, molecular recognition dyad self-assembles in solvents to form helically stacking structures have been described [36,37]. Notably, the chirality in the pendant tails is

* Corresponding author. Tel.: +357 90 392 630 1085; fax: +357 90 392 365 3641.
E-mail address: huriye.icil@emu.edu.tr (H. Icil).

0143-7208/$ – see front matter © 2009 Elsevier Ltd. All rights reserved.
doi:10.1016/j.dyepig.2009.04.014

crucial to control the chiroptical responses of the self-assembled structures [38–41]. Remarkably, use of chiral, self-assembled, donor and acceptor chromophores substituting fibers in optoelectronic devices, and prototypes and models for new nanoscale devices would lead to very exciting future applications. Transfer of chirality from low molecular chiral tectons to supramolecular assemblies has been presented [41]. Donor and acceptor chromophores on naphthalene and perylene diimide molecules revealed electron mobility via intra or intermolecular charge transfer interactions and electron transfer reactions [42–43]. Furthermore, results of similar studies on fluorophores conjugated DNA could be extremely important for environmental and biological applications [44].

In this paper, the synthesis of a novel naphthalene monoimide, N-(4-hydroxyphenyl)-1,4,5,8-naphthalenetetracarboxylic-1,8-anhydride-4,5-imide (**1**), as well as that of novel unsymmetrically substituted chiral naphthalene and perylene diimides **2** and **5**, N-(4-hydroxyphenyl)-N′-[(*S*)-1-phenylethyl]-1,4,5,8-naphthalenetetracarboxydiimide and N-(4-hydroxyphenyl)-N′-[(*S*)-1-phenylethyl]-3,4,9,10-perylenetetracarboxydiimide are reported and their photophysical, electrochemical, chiroptical and intramolecular charge transfer properties are explored; in addition, their solid state absorption are discussed. For comparison, perylene-3,4,9,10-tetracarboxylic acid monoanhydride monopotassium carboxylate (**3**) and N-(4-hydroxyphenyl)-3,4,9,10-perylenetetracarboxylic-3,4-anhydride-9,10-imide (**4**) were synthesized according to the methods given previously [11].

2. Experimental

2.1. Chemicals and instruments

1,4,5,8-naphthalenetetracarboxylic dianhydride, perylene-3,4,9,10-tetracarboxylic dianhydride, 4-aminophenol, potassium hydroxide, phosphoric acid and isoquinoline were obtained from Aldrich. (*S*)-(-)-α-methylbenzylamine, tetrabutylammonium hexafluorophosphate ($TBAPF_6$) and ferrocene were purchased from Fluka. All organic solvents employed were of spectroscopic grade.

IR spectra were measured as KBr pellets using a Mattson Sattelite FT-IR spectrometer. UV/vis spectra in solutions were recorded with a Varian-Cary 100 spectrometer. UV/vis spectra of solid state were measured in thin films using a Perkin–Elmer UV/VIS/NIR Lambda 19 spectrometer, equipped with solid accessories. Mass spectra were recorded with a Thermo Finnigan ESI instrument. Data were presented in *m*/*z* (%) values. Emission spectra were measured using a Varian-Cary Eclipse Fluorescence spectrometer. Optical rotations were measured with a Dr. Kernchen Sucromat digital automatic polarimeter, at 589 nm and 20 °C. CD spectra were measured on a JASCO 810 spectropolarimeter. Elemental analyses were obtained from a Thermo Finigann 1112C, H, N analyzer. ^{1}H and ^{13}C NMR spectra were measured with a Bruker AVANCE-500 spectrometer. Thermal analyses were recorded with a Perkin Elmer/Pyris 1. The samples were heated at 10 K/min. Cyclic and square-wave voltammetries in solvents were performed using a three-electrode cell with a polished 2 mm glassy carbon as working and Pt as counter electrode; solutions were 10^{-4} M in electroactive material and 0.1 M in supporting electrolyte, tetrabutylammonium hexafluorophosphate ($TBAPF_6$). Data were recorded on an EG&G PAR 273A computer-controlled potentiostat. Ferrocene was used as internal reference. The scan rate of 50–1000 mV^{-1} and the frequency 60–150 Hz were employed for cyclic and square-wave voltammetries, respectively. Cyclic and square-wave voltammetries in solid state were performed using an AUTOLAB system (Eco-Chemie, Utrecht, The Netherlands). The reference electrode was an Ag/AgCl electrode (saturated NaCl) with a potential of 0.200 V *vs*. SHE at 25 °C. A platinum wire served as an auxiliary electrode. A graphite rod (diameter: 0.5 cm) was used as working electrode. Compound was immobilized at the surface of the paraffin impregnated graphite electrodes (PIGEs) with a diameter of 5 mm. The solid compound was attached to the surface of PIGE by scratching. The supporting electrolyte was 1 M HCl. The scan rate of 25–600 mV^{-1} and the frequency 50–300 Hz were employed for solid state cyclic and square-wave voltammetries, respectively. Fluorescence lifetime measurement was performed by time correlated single photon counting technique (FLS920, from Edinburgh Instruments).

2.2. Novel synthetic compounds and procedures

The naphthalene monoimide (**1**) and two unsymmetric chiral diimides (**2**: naphthalene, **5**: perylene) were synthesized; for comparison purposes, the perylene monoimide (**4**) with the same substituent in naphthalene monoimide was prepared (Fig. 1). The unsymmetrical chiral naphthalene diimide was prepared using a two-step reaction process starting from 1,4,5,8-naphthalenetetracarboxylic dianhydride. In the first stage, *N*-(4-hydroxyphenyl)-1,4,5,8-naphthalenetetracarboxylic-1,8-anhydride-4,5-imide (**1**) was synthesized according to the literature [34]. In the final step, the chiral unsymmetrical naphthalene diimide (**2**) was synthesized via condensation of **1** with (*S*)-(-)-α-methylbenzylamine using *m*-cresol and isoquinoline as solvent mixture. The unsymmetrical chiral perylene diimide has been synthesized from perylene-3,4,9,10-tetracarboxylic dianhydride by a three-step reaction with the same amines (**5**). At the first and second steps, perylene-3,4,9,10-tetracarboxylic acid monoanhydride monopotassium carboxylate (**3**) and N-(4-hydroxyphenyl)-3,4,9,10-perylenetetracarboxylic-3,4-anhydride-9,10-imide (**4**) were synthesized and purified according to literature [21], respectively. Finally, the unsymmetrical chiral perylene diimide (**5**) was synthesized via condensation of (*S*)-(-)-α-methylbenzylamine with **4** using *m*-cresol and isoquinoline as solvent mixture.

2.2.1. N-(4-hydroxyphenyl)-1,4,5,8-naphthalenetetracarboxylic-1,8-anhydride-4,5-imide (**1**, Fig. 2)

Following the procedure of Ghadiri 1,4,5,8-naphthalenetetracarboxylic dianhydride (2.0 g, 7.5 mmol), water (350 mL) and KOH (1.0 M, 65 mL) were stirred for 2 h [34]. After the starting material had dissolved, the solution was acidified to pH 6.4 with H_3PO_4 (1.0 M). 4-Aminophenol (0.8 g, 7.5 mmol) was added and the solution was refluxed at 110 °C for 28 h. The solution was filtered, and the filtrate acidified with acetic acid (10%). The precipitate was collected by vacuum filtration, washed with water and dried in vacuum at 100 °C. The crude product was extracted with acetone in a Soxhlet apparatus during one day, in order to remove unreacted reactants. Yield (2.10 g, 78%); light-brown powder. FT-IR(KBr, cm^{-1}): ν = 3430, 1783, 1709, 1660, 1609, 1591, 1516, 1439, 1382, 1351, 1243, 1163, 1102, 956, 861, 824, 770, 646, 582, 535, 431. ^{1}HNMR, δ_H (ppm) (500 MHz, DMSO-d6): 8.51–8.49 (d, J = 6.7 Hz, 2 Ar-H, H-C(3), H-C(6)), 8.12–8.11(d, J = 7.0 Hz, 2 Ar-H, H-C(2), H-C(7)), 7.15–7.14 (app d, J = 7.7 Hz, 2 Ar-H, H-C(14), H-C(18)), 6.88–6.86 (app d, J = 7.7 Hz, 2 Ar-H, H-C(15), H-C(17)). ^{13}CNMR, δ_C (ppm) (100 MHz, DMSO-d6): 169.55 (2C═O, C(9), C(10)), 163.53 (2 C═O, C(11), C(12)), 157.33 (1(C), C(16)), 139.48 (1(C), C(13)), 130.22 (2 Ar-CH, C(2), C(7)), 129.94 (2 Ar-CH, C(3), C(6)), 128.94 (1(C), C(19)), 128.44 (2 Ar-CH, C(14), C(18)), 126.66 (2(C), C(1), C(8)), 125.68 (1(C), C(20)), 124.34 (2(C), C(4), C(5)), 115.54 (2 Ar-CH, C(15), C(17)). UV/Vis (DMF): λ_{max} (nm) (ε) = 356 (10850), 373 (11732). Fluorescence (DMF): λ_{max} (nm) = 407. Fluorescence quantum yield (MeOH, reference Anthracene with Φ_f = 27%, $\lambda_{exc.}$ = 360 nm) = 0.2%. MS (EI): *m*/*z*: 359 $[M]^+$. Anal. Calcd. for $C_{20}H_9NO_6$ (M_w, 359.3); C, 66.86; H, 2.52; N, 3.90. Found: C, 66.36; H, 2.54; N, 3.94.

2.2.2. N-(4-hydroxyphenyl)-N′-[(S)-1-phenylethyl]-1,4,5,8-naphthalenetetracarboxydiimide (**2**, Fig. 2)

N-(4-hydroxyphenyl)-1,4,5,8-naphthalenetetracarboxylic-1,8-anhydride-4,5-imide (1.0 g, 2.8 mmol), (*S*)-(-)-α-methylbenzylamine

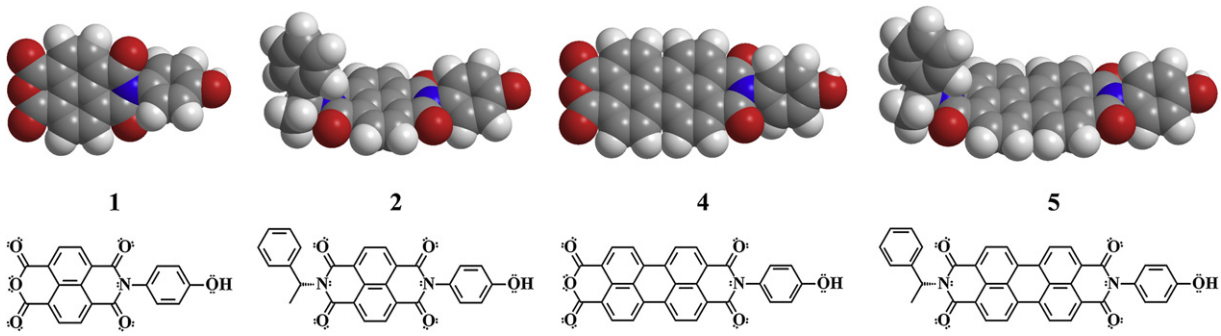

Fig. 1. **1**,**2**,**4** and **5** with a 3D model.

(1.1 mL, 8.4 mmol), m-cresol (40 mL) and isoquinoline (8 mL) were stirred under argon at 80 °C for 3 h, at 120 °C for 6 h, at 160 °C for 8 h and at 190 °C for 5h. The warm solution was poured into methanol (350 mL) and filtered. Hydrochloric acid (1.0 M) was added to the filtrate, and a brown solid precipitated from the solution. The product was further purified by crystallization from chloroform. The solid was collected by vacuum filtration, washed with water and dried in vacuum at 100 °C. Yield (1.10 g, 85%); brown powder. R_f (silica gel, $CHCl_3$) = 0.54. $[\alpha]_D^{20}$: −221.6 (c 0.0194, $CHCl_3$), FT-IR(KBr, cm^{-1}) : ν = 3430, 3053, 3026, 2976, 1708, 1660, 1611, 1590, 1513, 1450, 1350, 1326, 1250, 1195, 1102, 1066, 1030, 974, 876, 829, 769, 697, 568, 405. ^{1}HNMR, δ_H (ppm) (500 MHz, $CDCl_3$): 8.71–8.68 (d, 4 Ar-H, H-C(2), H-C(3), H-C(6), H-C(7)), 7.65–7.48 (m, 2 Ar-H, H-C(16), H-C(20)), 7.41–7.21 (m, 5 Ar-H, H-C(17), H-C(18), H-C(19), H-C(22), H-C(26)), 7.13–6.85 (m, 2 Ar-H, H-C(23), H-C(25)), 6.54–6.50 (q, J = 7.02, J = 7.005, J = 6.934, 1 C H, H-C(13)), 2.00–1.99 (d, J = 7.382, 1 CH_3, H_3-C(14)). ^{13}CNMR, δ_C (ppm) (100 MHz, $CDCl_3$): 163.35 (2 C=O, C(11), C(12)), 162.84 (2 C=O, C(9), C(10)), 157 (1(C), C(24)), 140.00 (1(C), C(15)), 139.9 (1(C), C(21)), 131.38 (2 Ar-CH, C(3), C(6)), 131.13 (2 Ar-CH, C(2), C(7)), 129.36 (1 Ar-CH, C(18)), 128.28 (2 Ar-CH, C(22), C(26)), 127.34 (2 Ar-CH, C(17), C(19)), 127.25 (2 Ar-CH, C(16), C(20)), 127.1 (1(C), C(27)), 126.9 (1(C), C(28)), 126.81 (2(C), C(4), C(5)), 126.5 (2(C), C(1), C(8)). UV/Vis (DMF): λ_{max} (nm) (ε) = 345 (13714), 360 (17918), 381 (18318). Fluorescence (DMF): λ_{max} (nm) = 410, 458, 500. Fluorescence quantum yield (DMF, reference Anthracene with Φ_f = 27%, $\lambda_{exc.}$ = 360 nm) = 0.8%. MS (EI): m/z: 463.5 $[M + 1]^+$. Anal. Calcd. for $C_{28}H_{18}N_2O_5$ (M_w, 462.5); C, 72.72; H, 3.92; N, 6.06. Found: C, 73.08; H, 4.02; N, 6.24.

2.2.3. *N-(4-hydroxyphenyl)-N′-[(S)-1-phenylethyl]-3,4,9,10-perylenetetracarboxydiimide (**5**, Fig. 3)*

N-(4-hydroxyphenyl)-3,4,9,10-perylenetetracarboxylic-3,4-anhydride-9,10-imide (0.4 g, 0.8 mmol), (*S*)-(-)-α-methylbenzylamine (0.2 mL, 1.8 mmol) and isoquinoline (40 mL) were stirred under argon at 60 °C for 2h, at 80 °C for 3 h, at 120 °C for 8 h, at 160 °C for 10 h, at 180 °C for 8 h and at 200 °C for 18 h. The warm solution was poured into methanol (300 mL). The precipitate was collected by vacuum filtration, washed with water and dried in vacuum at 100 °C. The crude product was extracted for 24 h with methanol then ethanol in order to remove high boiling solvents and the unreacted reactants using a Soxhlet apparatus. Yield (0.45 g, 92%); black-brownish powder. R_f (silica gel, $CHCl_3$) = 0.25. $[\alpha]_D^{20}$: −24 (c 0.052, DMSO). FT-IR(KBr, cm^{-1}) : ν = 3370, 3063, 3025, 2966, 2926, 1698, 1659, 1594, 1577, 1513, 1449, 1403, 1354, 1256, 1179, 1124, 960, 837, 810, 746, 697, 601, 531, 490, 430. ^{1}HNMR, δ_H (ppm) (400 MHz, Pyridine-d5) = 8.92–8.48 (m, 8 Ar-H, H-C(1), H-C(2), H-C(5), H-C(6), H-C(7), H-C(8)), 7.79–7.69 (m, 4 Ar-H, H-C(18), H-C(19), H-C(21), H-C(22)), 7.43–7.25 (m, 5 Ar-H, H-C(26), H-C(27), H-C(28), H-C(29), H-C(30)), 6.98 (s, 1 OH, HO-C(20)), 6.85–6.80 (q, J = 7.09, 1 CH, H-C(23)), 2.18–2.16 (d, J = 6.85, 1CH_3, H_3-C(24)). UV/Vis (DMF): λ_{max} (nm) (ε) = 459 (40606), 490 (58 465), 526 (70 000). Fluorescence (DMF): λ_{max} (nm) = 539, 580. Fluorescence quantum yield (MeOH, reference N, N′-didodecyl-3,4,9,10-perylenebis(dicarboxiimide) with Φ_f = 100%, $\lambda_{exc.}$ = 485 nm) = 80%. MS (EI): m/z: 587.5 $[M + 1]^+$. Anal. Calcd. for $C_{38}H_{22}N_2O_5$ (M_w, 586.6); C, 77.81; H, 3.78; N, 4.78. Found: C, 77.52; H, 3.64; N, 4.43.

3. Results and discussion

3.1. *Synthesis and characterization of naphthalene and perylene monoimides (**1**, **4**) and diimides (**2**, **5**)*

Unsymmetrically substituted chiral naphthalene and perylene diimides (**2**, **5**) were prepared according to the synthetic routes shown in Figs. 2 and 3, respectively. The diacid naphthalenetetracarboxylic acid monoanhydride was directly converted to naphthalene monoimide (**1**) via condensation with 4-aminophenol at 110 °C for 10 h (Fig. 2). Compounds **3** and **4** were synthesized according to the methods given in our previous works [11,17]. The structures of the compounds were characterized by ^{1}HNMR, ^{13}CNMR, MS, IR and elemental analysis; the results clearly support the predicted chemical structures of all the compounds (Fig. 1).

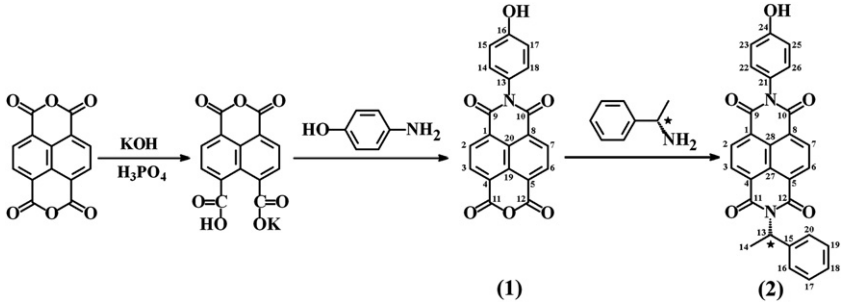

Fig. 2. Synthesis of naphthalene monoimide (**1**) and unsymmetrical chiral naphthalene diimide (**2**).

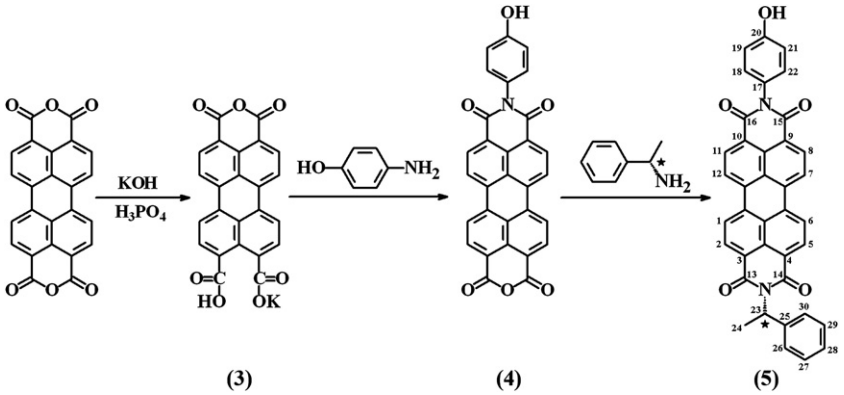

Fig. 3. Synthesis of perylene-3,4,9,10-tetracarboxylic acid monoanhydride monopotassium carboxylate (**3**), perylene monoimide (**4**) and unsymmetrical chiral perylene diimide (**2**).

All IR spectra were consistent with the assigned structures as shown in Figs. 2, 3 and 4. The IR spectrum of **1** exhibited characteristic absorption bands at 3430 (O–H stretch); 1783 (anhydride C═O stretch); 1709, 1660 (imides C═O stretch); 1609, 1591 (conjugated C═C stretch); 1351 (C-N stretch); 1102 (C–O–C stretch); 861 and 770 (C–H bend) cm^{-1}. In the IR spectrum of 2, the characteristic bands of the anhydride carbonyl stretching bands (1783 cm^{-1}) had disappeared and were replaced by the *N*-imide carbonyl stretching bands (1708 and 1660 cm−1). Similarly, the characteristic band of the C–O–C stretching (1102 cm^{-1}) had disappeared and was replaced by C–N stretching band (1350 cm^{-1}). Other absorption bands of **2** were very similar to those of **1** (Fig. 4(a)). The IR spectrum of **4** exhibited characteristic absorption bands at 3443 (O–H stretch); 3096 (aromatic C–H stretch); 1773, 1730 (anhydride C═O stretch); 1698, 1659 (imides C═O stretch); 1594 (conjugated C═C stretch); 1300 (C–N stretch); 1025 (C–O–C stretch); 808 and 732 (C–H bend) cm^{-1}. In the IR spectrum of **5**, the characteristic bands of the anhydride carbonyl stretching bands (1773 and 1730 cm^{-1}) had disappeared and were replaced by N-imides carbonyl stretching bands (1698 and 1659 cm^{-1}). Similarly, the characteristic band of the C–O–C stretching (1025 cm^{-1}) had disappeared and was replaced by C–N stretching band (1354 cm^{-1}). An additional band appeared at 2926 cm^{-1} due to aliphatic C–H stretching. Other absorption bands of **5** were very similar to those of **4** (Fig. 4(b)).

Table 1 lists the solubility properties of **1**, **2**, **4** and **5**. Solubility of monoimides is lower than that of diimides which is depended on intermolecular interactions that are affected by the rigidity and symmetry. The presence of secondary carbon atoms next to nitrogen atoms force the methyl and phenyl substituent out of the plane of the molecule and thereby hamper the face-to-face π–π stacking of the **2** and **5** [21]. The sterically hindered chiral substituent prevented the short π–π contacts of the fluorophores and resulted in higher solubility. With less rigid **2**, these effects are more pronounced comparing to **5** which contribute to the higher solubility. Similarly, chiral **5** was poorly soluble compared to our previously reported symmetrically substituted chiral perylene diimide [21].

The main fragmentation routes of the compounds **1**, **2** and **5** are shown in Fig. S1. The mass spectrum of the compound **1** showed the corresponding molecular ion peak at 359 *m*/*z*, which was also the base peak. The fragment of 250 *m*/*z* was produced by the breakage of C_6H_4NO

(Fig. S1(a)). The base peak again coincided with the molecular ion peak for compound **2** at 463.5 *m*/*z* (M + 1) (Fig. S1(b)). The fragment of 372.4 *m*/*z* was produced by the breakage of C_7H_7 (Fig. S1(b)). The mass spectrum of **5** (Fig. S1(c)) showed the corresponding molecular ion peak at 587.5 *m*/*z* (M + 1). The base peak occurred at 302.3 *m*/*z* was produced by the cleavage of $C_{16}H_{17}N_2O_3$.

3.2. Absorption and fluorescence properties

The absorption and emission spectra of **1** in non-polar, polar protic and aprotic solvents are shown in Fig. 5(a): absorption spectra at 10^{-5} M concentration, (b): absorption spectra of filtered solution through a 0.2 μm SPR microfilter, (c): emission spectra at 10^{-5} M concentration, (b): emission spectra of filtered solution through a 0.2 μm SPR microfilter. The absorbance is significantly dependent on the solubility of the compound and the polarity of

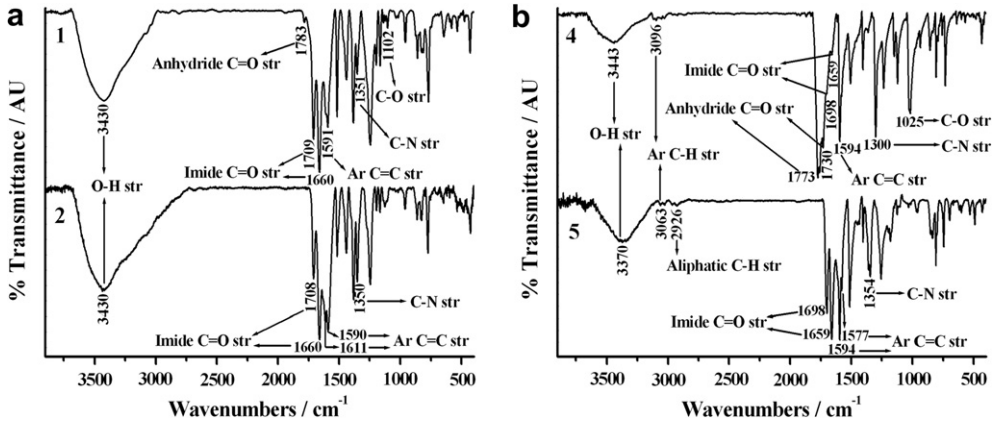

Fig. 4. FT-IR spectra of (a) **1** and **2**; (b) **4** and **5**.

Table 1
Solubility of **1**, **2**, **4** and **5**.

	Solubility[a]/Colour			
	1	2	4	5
$CHCl_3$	+ - Colorless	+ Brown	-	+ - Orange
DCM	+ - Colorless	+ Brown	-	+ - Orange
Pyridine	+ - Colorless	+ Brown	-	+ Yellow
Acetone	+ - Colorless	+ Brown	-	+ - Yellow
EtOH	+ - Colorless	+ Brown	-	+ - Yellow
NMP	+ - Pale Yellow	+ Brown	+ Red	+ Red
MeOH	+ - Colorless	+ Brown	-	+ - Yellow
CH_3CN	+ - Colorless	+ Brown	-	+ - Yellow
DMF	+ Pale Yellow	+ Brown	+ Red	+ - Light Pink
DMSO	+ Pale Yellow	+ Brown	+ Red	+ - Red
H_2O	+ - Colorless	-	-	-

- insoluble at RT. DCM: dichloromethane; NMP: N-methylpyrrolidinone. DMF: dimethylformamide; DMSO: dimethyl sulfoxide.
[a] 0.1 mg in 1.0 mL of solvent. + soluble; + - partially soluble.

solvent. Characteristically three absorption bands are observed in solvents (non-polar and polar) where compound **1** dissolves rather poorly such as $CHCl_3$, DCM and CH_3CN (in $CHCl_3$: 334, 350 and 370 nm) which is in agreement with literature data for other naphthalene diimides [4]. The broad long wavelength absorption band of **1** in polar solvents EtOH, NMP, MeOH, DMF, DMSO and H_2O presents a solvent dependent charge transfer character corresponding to a shift of the electron density from the electron rich moiety (hydroxyl substituent) towards the imide carbonyls and it is significantly red shifted compared to the bands in $CHCl_3$, DCM and CH_3CN solvents (Fig. 6(a) and (b)). On the other hand, the lack of a charge transfer band in the polar solvent acetonitrile is attributed to the rather poor solubility of compound **1** in this solvent. The extension of the π conjugation system accounts for the narrowing of the HOMO-LUMO gap in the compound **1**. Additionally, the lower degree of symmetry of **1** may induce a higher number of vibronic modes which results in a broader absorption band. The small changes on absorption bands regarding to their initial shape upon filtration of the solutions through a 0.2 μm SPR microfilter (Fig. 5(b)) indicate weak aggregated distributions in polar solvents except $CHCl_3$, DCM and CH_3CN. The absorption and emission spectra of **2**, **4** and **5** in the same non-polar, polar protic and aprotic solvents used in the electronic spectra of **1** are shown in Fig. 6 (**2**; (a): absorption spectra at 10^{-5} M concentration, (b): absorption spectra of filtered solution through a 0.2 μm SPR microfilter, (c): emission spectra at 10^{-5} M concentration, (d): emission spectra of filtered solution through a 0.2 μm SPR microfilter) and S2 (**4**; (a): absorption spectra at 10^{-5} M concentration, **4**; (b): emission spectra at 10^{-5} M concentration, **5**; (c): absorption spectra at 10^{-5} M concentration, **5**; (d): emission spectra at 10^{-5} M concentration). In contrast to **1** the compounds **2**, **4** and **5** exhibit the characteristic three absorption bands of the compound class in their absorption spectra (solvent: DMSO; **2**: 345, 360, 381 nm; **4** : 454, 482, 518 nm and **5** : 461, 492, 529 nm) indicating the absence of a strong charge-transfer interaction in the ground state. The values of the absorption wavelength maxima for all solvents are nearly the same without charge transfer complexation. Consequently, there is more intensive interaction between **1** and solvent molecules so as to influence its shape of absorption spectra which is not observed for **2**, **4** and **5**.

Interestingly, all the emission spectra of **1** and **2** show characteristically red shifted and broad excimer-like emissions (Figs. 5 and 6; $\lambda_{exc} = 360$ nm) which have been thought as important indication of weakly interacting π-stacks in solutions. The higher Stokes shift (Figs. 5 and 6, Table 2; **1**: 123 457 cm^{-1}, filtered solution through a 0.2 μm SPR microfilter (**1***): 138 889 cm^{-1}, **2**: 120 482 cm^{-1} and filtered solution through a 0.2 μm SPR microfilter (**2***): 121 951 cm^{-1})

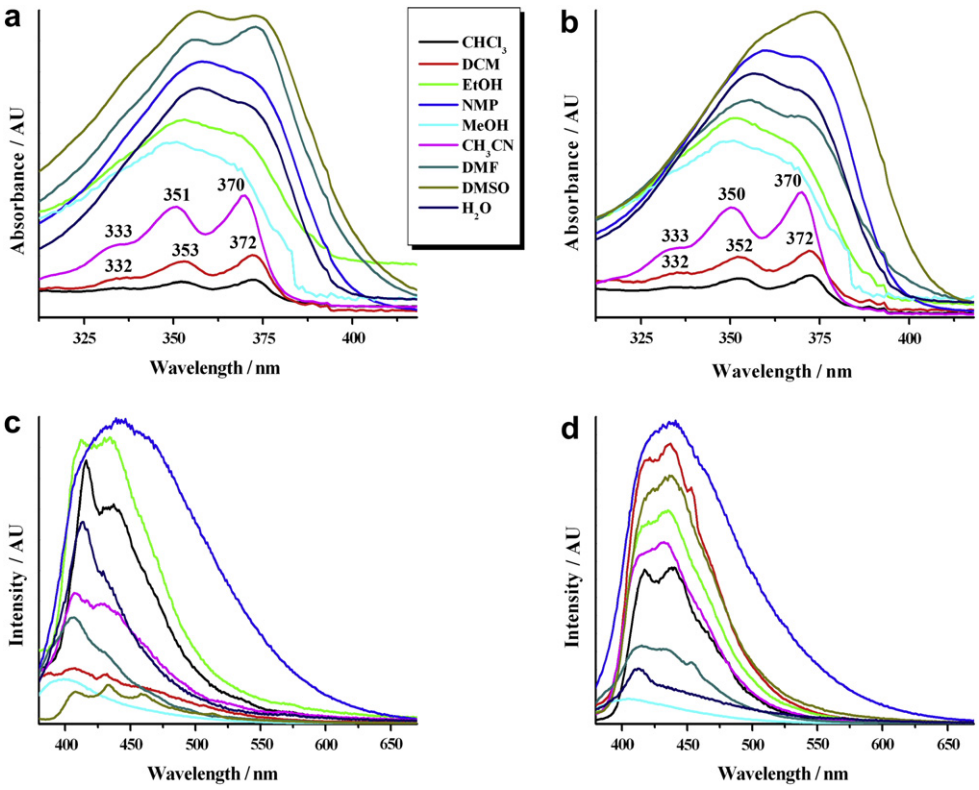

Fig. 5. (a) Absorption spectra of **1** in different solvents; (b) after filtration with 0.2 μm microfilter; (c) emission spectra of **1** in different solvents at the excitation wavelength 360 nm; (d) after filtration with 0.2 μm microfilter.

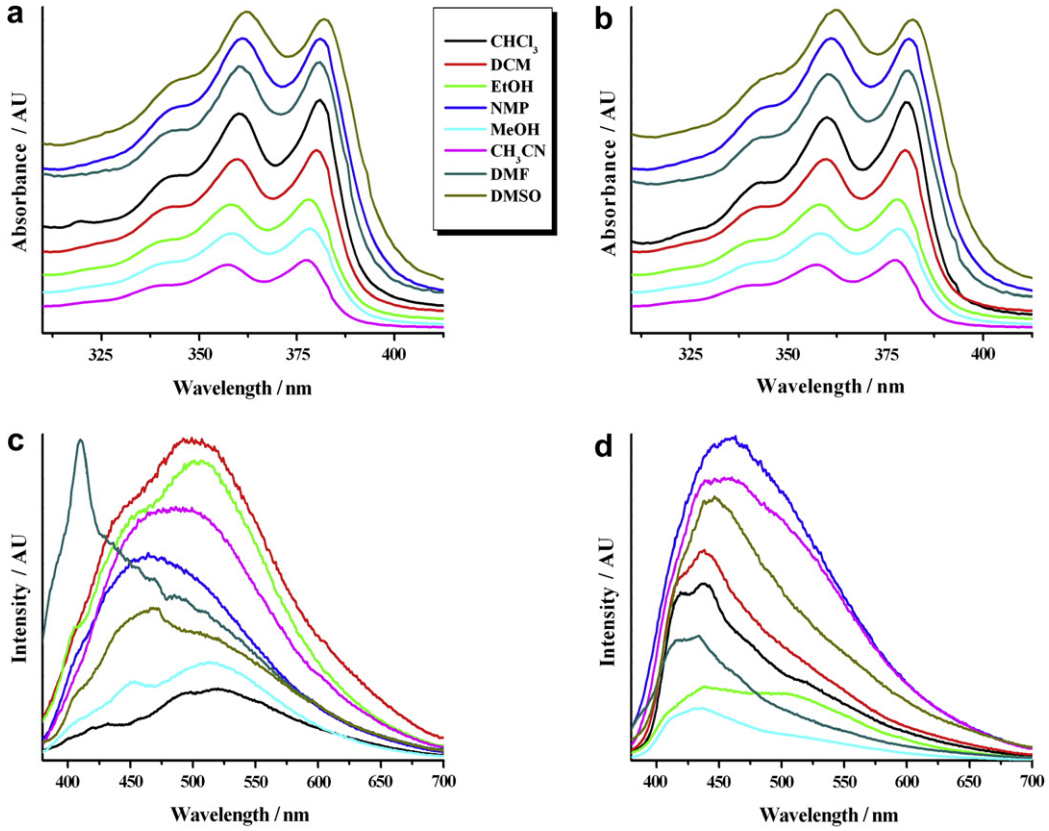

Fig. 6. (a) Absorption spectra of **2** in different solvents; (b) after filtration with 0.2 μm microfilter; (c) emission spectra of **2** in different solvents at the excitation wavelength 360 nm; (d) after filtration with 0.2 μm microfilter. These spectra are offset in the ordinate for clarity.

value and broadest band for the spectrum taken in NMP showed the presence of a relatively large amount of non-radiative energy lost. The difference in Stoke shift between the solution taken at 10^{-5} M concentration and filtered solution through a 0.2 μm SPR microfilter was attributed to weak aggregation (Table 2). The emission spectra of **1** and **2** were very similar to the excimer-like emissions usually observed for π-stacked interacting molecules in solution. Besides the well resolved absorption bands for **2**, the excimer-like emission of the compound has been thought as an important indication of weaker interacting π-stacks in solution. Additionally, the shape of the emission spectra and obtained peak maxima upon filtration of the solutions through a 0.2 μm SPR microfilter (Figs. 5 and 6(c) and (d)) indicates aggregated emission besides the excimer emission in the excited state. The fluorescence spectra of **4** and **5** taken at $\lambda_{exc} = 485$ nm showed mirror images of their absorption spectra with small Stokes shifts and the absence of excimer emission (Fig. S2, Table 2; **4** and **5**: 1 000 000–666 667 cm^{-1} before and after filtration). All these unique properties indicate the similarity between ground S_0 and excited S_1 states. As expected, dominance of rigidity and planarity gave a small Stokes shift and greater reabsorption.

The emission spectra of compounds **1** and **2** were taken at $\lambda_{exc} = 360$ nm and the relative fluorescence quantum yields were determined in DMF by using anthracene as a standard in EtOH. The low fluorescence quantum yields of **1** and **2** are in good correlation with literature data (**1**: 0.2% and **2**: 0.8%) [4]. The emission spectra of **4** and **5** was taken at $\lambda_{exc} = 485$ nm and the relative fluorescence quantum yields determined in DMF using *N*,*N*́-didodecyl-3,4,9,10-perylenebis(dicarboximide) in $CHCl_3$ as standard. The lower fluorescence quantum yield of **4** could be attributed to conformational changes, torsional movement, or other non-radiative decays (**4**: 60% and **5**: 80%).

Fig. 7 shows the absorption spectra of **1**, **2**, **4** and **5** in the solid state and Table 3 provides a summary of the experimental spectroscopic

Table 2
Stokes shifts of **1**, **2**, **4** and **5**.

	Stokes Shift (cm^{-1})							
	1	1*	2	2*	4	4*	5	5*
$CHCl_3$	227273	222222	200000	256410	–	–	1000000	1000000
DCM	285714	204082	84034	172414	–	–	909091	909091
EtOH	169492	144928	81301	166667	–	–	714286	714286
NMP	123457	138889	120482	121951	666667	666667	769231	769231
MeOH	208333	277778	133333	192308	–	–	666667	666667
CH_3CN	270270	161290	91743	120482	–	–	769231	769231
DMF	294118	217391	344828	250000	666667	666667	769231	769231
DMSO	285714	200000	120482	156250	833333	833333	714286	714286
H_2O	178571	232558	–	–	–	–	–	–

*after filtration with 0.2 μm microfilter.

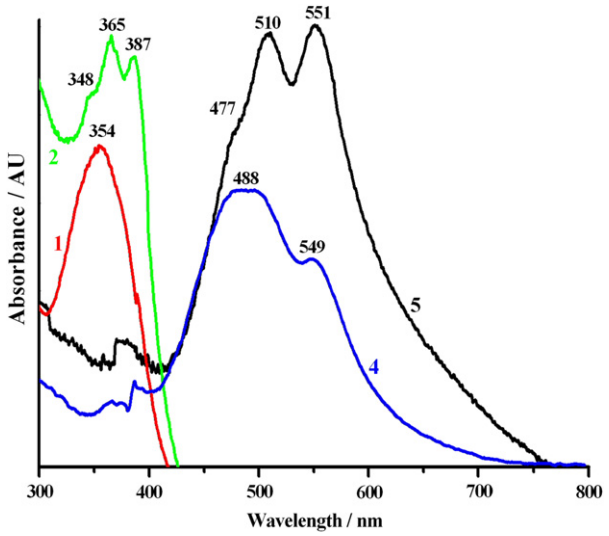

Fig. 7. Solid state UV/vis absorption spectra of **1**, **2**, **4** and **5**.

data for them together with calculated values. An intermolecular electron–donor–acceptor complex are formed for **1** in the solid state which gives rise to an intermolecular charge transfer absorption at 354 nm as an unresolved band. The main difference between the uv spectra in solid and solution states of **1** is the shoulder around 373 nm in the solution spectra. Interestingly, the solid state uv spectra of **1**, and **2** are very similar to their spectra taken in solution which indicate weakly interacting π-stacks in solid state and similar intermolecular interactions in both states. It is worth noting that the solid state spectra of **4** and **5** are different with respect to the absorption maxima and band shapes which indicate different π interaction in solid state. A higher red shift of the 0–0 band was observed for **4** due to the stronger intermolecular π-stacking interactions (for the filtered solutions through a 0.2 μm SPR microfilter; **4**: 31 nm and **5**: 25 nm in DMF). Solid state fluorescence of all the compounds could not be obtained which is attributed to presence of aggregates and excimers, which normally reduce quantum efficiencies of emission in the solid state. Maximum absorption wavelengths (λ_{max} in nm), extinction coefficients (ε_{max}), oscillator strengths *f*, fluorescence quantum yields (Φ_f), radiative lifetimes τ_0 (ns), fluorescence lifetimes τ_f (ns), fluorescence rate constants k_f, rate constant of radiationless deactivation k_d, optical activity and singlet energies E_s (kcal mol^{-1}) data of all the compounds in DMF, are given in Table 3. Notably, the high solvent sensitivity of the emissions of compounds **1** and **2** indicates a polar character for the emitting species. The excimer-like emissions and the low fluorescence quantum rate constant in DMF supports the charge transfer complexes in solutions as well. The fluorescence lifetime of **1** and **2** are calculated as 10 and 30 ps respectively, which support the ultra fast intersystem crossing from the singlet excited state. We were unable to measure fluorescence lifetimes of the compounds which are shorter than the resolution times of our equipment (100 ps). The fluorescence lifetime of **4** and **5** is observed experimentally as 3.9 and 4.2 ns, respectively (λ_{exc} = 530 nm, Fig. 8). The singlet energies were calculated in kcal mol^{-1} using equation $E_s = 2.86 \times 10^5/\lambda_{max}$, where λ_{max} stands for maximum absorption wavelength in angstroms [45]. The theoretical radiative lifetimes τ_0 were calculated according to the formula: $\tau_0 = 3.5 \times 10^8/(\nu^2_{max} \times \varepsilon_{max} \times \Delta\nu_{1/2})$, where ν_{max} stands for the wavenumber in cm^{-1}, ε_{max} for the molar extinction coefficient at the selected absorption wavelength and $\Delta\nu_{1/2}$ indicates the half-width of the selected absorption in units of cm^{-1} [45]. Fluorescence lifetimes were calculated from $\tau_f = \tau_0 \times \Phi_f$ and the rates of fluorescence from $k_f = 1/\tau_0$ (Table 3). The radiationless deactivation rate constants were calculated from $k_d = (k_f/\Phi_f) - k_f$ and oscillator strength from $f = 4.32 \times 10^{-9} \times \Delta\nu_{1/2} \times \varepsilon_{max}$ [45]. The technique of time correlated single photon counting was used to record fluorescence lifetimes of the compounds. The decay curves were multi-exponential and analysed by using the standard method of iterative reconvolution and non-linear least square fitting method (Fig. 8). The quality of calculated fits was judged using statistical parameters, the reduced χ^2 value and the residual data. Experimental radiative lifetimes, fluorescence lifetimes, fluorescence rate constants, rate constant of radiationless deactivation, and singlet energies data of all the compounds in DMF were consistent with literature data [11].

The specific optical rotation ($[\alpha]_D^{20}$, alpha) of **2** and **5** measured at 20 °C (Solvent: DMF; **2**: c = 0.0194 mg mL^{-1} in and **5**: c = 0.052 mg mL^{-1}) as −221.6 and −24, respectively. Fig. 9 shows the CD spectra of **2** in acetonitrile and ethanol, respectively. Compound **2** showed a prominent negative Cotton effect which corresponds to the maximum absorption bands in the UV spectra recorded (acetonitrile: 362 and 382 nm, ethanol: 364 and 384 nm). No significant spectroscopic changes were observed in these two solvents. The CD signal provides support for the helical conformation of the synthesized compound. However no detectable Cotton effect was obtained for compound **5**, a feature which is probably due to the poor solubility comparing to compound **2** in solution at room temperature.

3.3. Thermal stability

The thermal behavior of **1**, **2** and **5** was investigated by DSC and TGA (TGA: heating rate 5 K min^{-1}, DSC: heating rate 10 K min^{-1}, Fig. 10 and S3). All compounds exhibit no glass transition temperature in the DSC run (**1** and **2**: 0–300 °C and **5**: 0–400 °C). The curves showed the high decomposition temperatures (T_d) for the compounds. Compounds **1**, **2** and **5** were stable up to 323, 353 and 373 °C, respectively. For compound **1**, a rapid weight loss of 70% of the initial weight was occurred between 323 and 415 °C. When **1** was heated to 900 °C, 91% of the initial weight was lost, and about 9% char yield observed. For compound **2**, a rapid weight lost of 27% of the initial weight occurred between 353 and 405 °C When **2** was heated to 650 °C, 98% of the initial weight was lost rapidly and about 2% char yield observed. Compound **2** showed higher thermal stability than compound **1** that could be attributed to the intermolecular forces, rigidity and symmetry of the structure. For compound **5**, a rapid

Table 3
Maximum absorption wavelengths λ_{max} (nm), extinction coefficients ε_{max} (l mol^{-1} cm^{-1}), oscillator strengths f, fluorescence quantum yields Φ_f ($\lambda_{exc.}$ = 360 nm for OH-NMI and HC-NDI, $\lambda_{exc.}$ = 485 nm for HC-PDI), radiative lifetimes τ_0 (ns), fluorescence lifetimes τ_f (ns), fluorescence rate constants k_f (10^8 s^{-1}), rate constants of radiationless deactivation k_d (10^8 s^{-1}), optical activities $[\alpha]_D^{20}$, and singlet energies E_s (kcal mol^{-1}) data of **1**, **2**, **4** and **5** in DMF.

	λ_{max}	$\lambda_{max\ (solid\ state)}$	ε_{max}	f	Φ_f	τ_0	τ_f	k_f	k_d	$[\alpha]_D^{20}$	E_s
1	373	354	11 732	0.4	0.002	5.34	0.01	1.9	948	–	76.7
2	381	387	18 318	0.6	0.008	3.63	0.03	2.8	341	−221.6	75.1
4[a]	518	488	71 000	0.3	0.60	13.4	8.04 (3.9)	0.7	0.5	–	55.2
5[a]	526	551	70 000	0.4	0.80	10.6	8.48 (4.2)	0.9	0.2	−24	54.4

[a] Experimental values are given in parantheses.

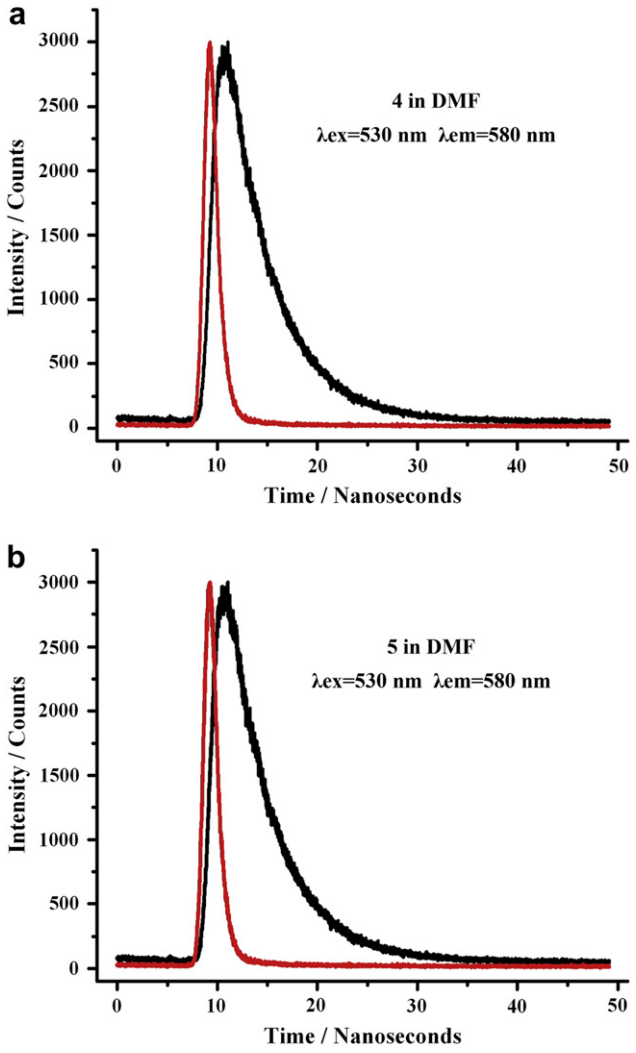

Fig. 8. Fluorescence decay curves of (a) 10^{-5} M **4**; (b) 10^{-5} M **5** ($\lambda_{exc.}$ = 530 nm and λ_{em} = 580 nm) in DMF.

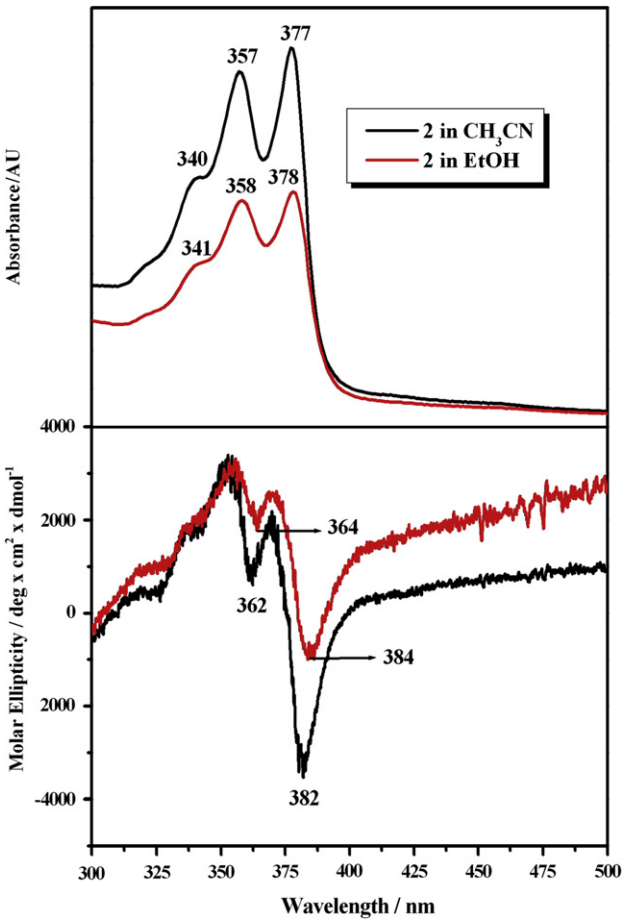

Fig. 9. CD spectra of **2** in acetonitrile and ethanol.

weight lost of 20% of the initial weight occurred between 373 and 423 °C. When **5** was heated to 900 °C, 44% of the initial weight was lost, and about 56% char yield observed. Accordingly, **5** showed highest thermal stability that could be attributed to the intermolecular forces, rigidity and symmetry of the structure. Remarkably, the compound **5** showed better thermal stability at elevated temperature (symmetrical PDI: 2% char yield at 900 °C) with higher char yield compared with the symmetrical PDI bearing the same chiral substituent.

3.4. Electrochemistry

The electrochemical characterization of all compounds were studied in detail using cyclic (CV: **1**, **2** and **5**) and square-wave (SWV: **5**) voltammetries in different solvents containing 0.1 M $TBAPF_6$ as a supporting electrolyte and in solid state (Figs. 11 and 12) which summarized in Table 4, S1 and S2. Due to the poor solubility of **4** in general organic solvents its electrochemical characterization could not be determined. All the measured redox potentials, HOMO (highest occupied molecular orbital)/LUMO (lowest unoccupied molecular orbital) and band gap energy E_g values obtained from those are tabulated in Table 4. All compounds undergo two reversible one-electron reductions, the first of which is the reduction of the neutral compound to radical anion ($\mathbf{1}^-$, $\mathbf{2}^-$ and $\mathbf{5}^-$) and the second reduction corresponds to the formation of the dianion ($\mathbf{1}^{2-}$, $\mathbf{2}^{2-}$and $\mathbf{5}^{2-}$) as shown in Fig. 13. Similarly, for compounds **1**, **2** and **5** the values of the half-wave potential ($E_{1/2}$) were found to be independent of the scan rate, as was expected for a reversible system.

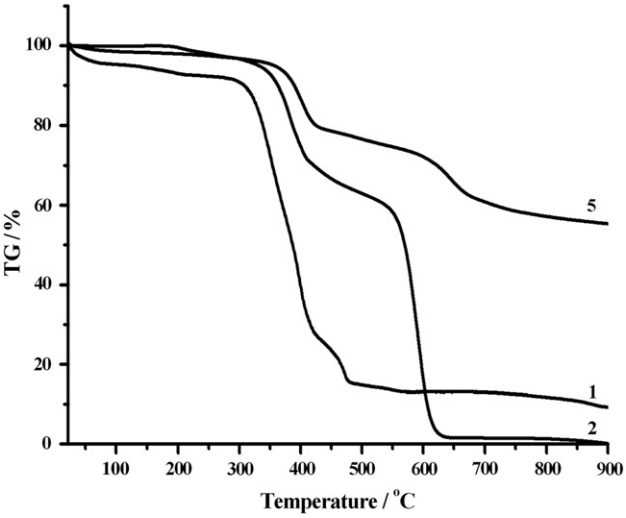

Fig. 10. Thermal gravimetric analysis (TGA) of compounds **1**, **2**, and **5**.

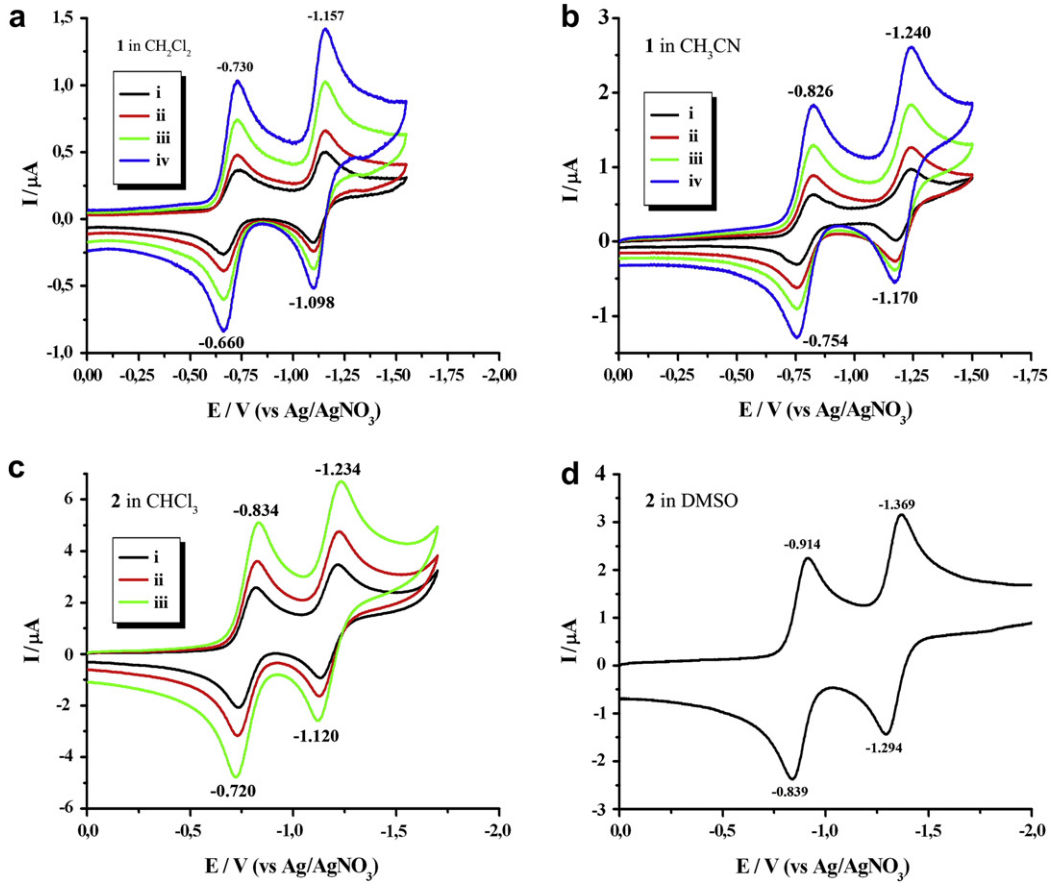

Fig. 11. Cyclic voltammograms of (a) **1** in dichloromethane; (b) **1** in acetonitrile, scan rates (mVs^{-1}): i (50), ii (100), iii (200), iv (300); (c) **2** in chloroform, scan rates (mVs^{-1}): i (50), ii (100), iii (200); (d) **2** in DMSO, scan rate (mVs^{-1}): 50, supporting electrolyte: $TBAPF_6$.

As shown in Figs. 11 and 13, cyclic voltammogram of compound **1** has shown two fast reversible, one-electron reductions at −0.695 and −1.127 V (vs. $Ag/AgNO_3$, scan rate: 100 mV s^{-1}) with peak potential separations $\Delta E_{p1} = 67$ mV and $\Delta E_{p2} = 60$ mV, respectively in CH_2Cl_2 (Fig. 11(a) and Table 4). The calculated ΔE_p in the range 60–70 mV for **1** shows that reversibility of electron transfer was fairly well maintained in this system. The reduction couples for **1** were observed at $E_{1/2} = -0.790$ and −1.205 V (vs. $Ag/AgNO_3$, scan rate: 100 mV s^{-1}) in more polar solvent CH_3CN (Fig. 11(b) and Table S1, $\Delta E_{p1} = 68$ mV and $\Delta E_{p2} = 68$ mV). Compound **2** displays two fast reversible one-electron reductions at −0.776 and −1.176 V (vs. $Ag/AgNO_3$, scan rate: 100 mV s^{-1}) with peak potential separations $\Delta E_{p1} = 97$ mV and $\Delta E_{p2} = 99$ mV, respectively in $CHCl_3$ (Fig. 11(c) and Table 4). These values were observed at −0.777 and −1.175 V at scan rate of 50 mV s^{-1} with peak potential separations $\Delta E_{p1} = 86$ mV and $\Delta E_{p2} = 87$ mV. The reduction couples for **2** were observed at $E_{1/2} = -0.876$ and −1.331 V (vs. $Ag/AgNO_3$, scan rate: 50 mV s^{-1}) in the more polar solvent DMSO (Fig. 11(d) and Table S1, $\Delta E_{p1} = 75$ mV and $\Delta E_{p2} = 75$ mV). Notably, $E_{1/2}$ shifts towards high negative potentials in more polar solvents indicating a more difficult reduction probably due to the stable complex formation (**1**: CH_2Cl_2 and CH_3CN, **2**: $CHCl_3$ and DMSO, Table S1).

In order to calculate the absolute energies of LUMO level of **1** and **2** with respect to the vacuum level, the redox data are standardized to the ferrocene/ferricenium couple which has a calculated absolute energy of −4.8 eV [46,47]. The LUMO energies of the **1** and **2** were calculated from cyclic voltammograms (Fig. 11 and Table 4) as −3.93 and −3.79 eV, respectively. The optical band gap, E_g values, were calculated to be approximately 3.21 and 3.15 eV for the compound **1** and **2**, respectively where E_g was obtained from the edge of the electronic absorption band with $E_g\,(eV) = hc/\lambda$ ($h = 6.626 \times 10^{-34}$ J s, $c = 3 \times 10^{10}$ cm s^{-1}, 1 eV = 1.602×10^{-19} J). From this value, the HOMO energies of **1** and **2** were estimated from the relationship $E_{HOMO} = E_{LUMO} - E_g$, as −7.14 and −6.94 eV, respectively.

The electrochemical stability and reversibility of the redox processes of **1** and **2** were examined using cyclic voltammetry (Fig. 11 and Table S1) in different solvents (**1**: CH_2Cl_2 and CH_3CN, **2**: $CHCl_3$). Electrochemical stability of the compounds was examined by measuring repeated cycles of redox processes. Compound **1** showed completely reversible reduction steps for the entire scanning rate in a region of 50–300 mV s^{-1}. As shown in Table S1, the ΔE_p was about 59–78 mV for each cycle of **1** in CH_2Cl_2. Similar results were attained with the solvent CH_3CN. Compound **2** showed completely reversible reduction steps for the entire scanning rate in a region of 50–200 mV s^{-1}. At the large ΔE_p values (114 mV at 200 mV s^{-1}), which indicate the limitation due to charge transfer kinetics, the reversibility of the compound **2** was poor. According to standard reversibility criteria, each reduction process indicates reversible, diffusion-controlled one-electron transfer. A plot of peak current against square root of scan rate was found to be linear as shown in Fig. S4 for compounds **1** and **2** (**1**: in CH_2Cl_2 $R^2 = 0.99$ and CH_3CN $R^2 = 0.98$, **2**: in $CHCl_3$ $R^2 = 1.00$), which fulfills the conditions for diffusion-controlled processes.

The diffusion coefficients D were measured by cyclic voltammetry according to Randles-Sevcik equation [48]: $i_p = (2.69 \times 10^5) \times n^{3/2} \times v^{1/2} \times D^{1/2} \times A \times C$, where i_p is peak current (A), n is the number of

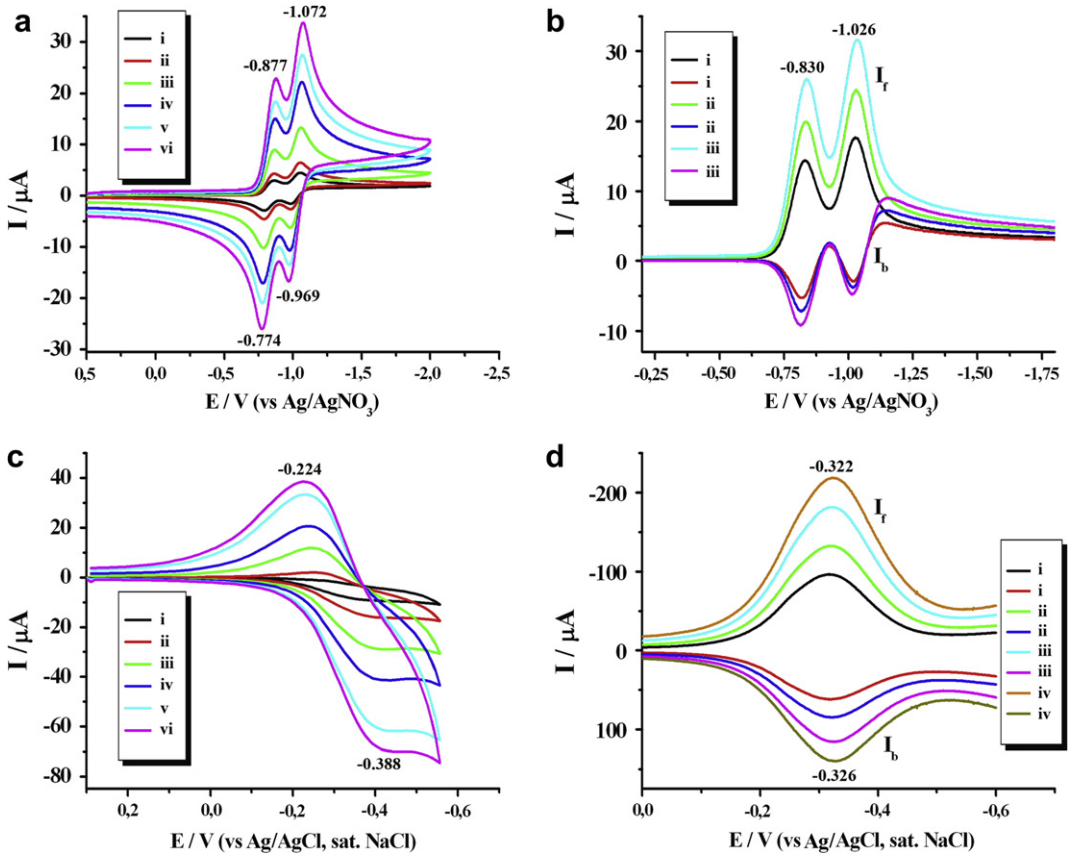

Fig. 12. (a) Cyclic voltammograms of **5** in chloroform; supporting electrolyte: $TBAPF_6$, scan rates (mVs^{-1}): i (50), ii (100), iii (300), iv (600), v (800), vi (1000); (b) square-wave voltammograms of **5** in chloroform; supporting electrolyte: $TBAPF_6$, ν (Hz): i (60), ii (100), iii (150); (c) solid state cyclic voltammograms of **5**; supporting electrolyte: HCl, scan rates (mVs^{-1}): i (25), ii (50), iii (100), iv (200), v (400), vi (600); (d) solid state square-wave voltammograms of **5**; supporting electrolyte: HCl, ν (Hz): i (50), ii (100), iii (200), iv (300) at 25 °C.

transferred electrons, v is the scan rate (V s^{-1}), D is the diffusion coefficient (cm^2 s^{-1}), A is the electrode area (cm^2), C is the concentration of the electroactive species (mol cm^{-3}). The diffusion coefficients (D) of **1** and **2** in solution were estimated from the slope of the plot i_{pc} versus $v^{1/2}$ (Fig. S4). Accordingly, the diffusion coefficients were determined as 8.73×10^{-8} and 2.55×10^{-7} cm^2 s^{-1} for **1** in CH_2Cl_2 and CH_3CN, respectively, and 2.63×10^{-6} cm^2 s^{-1} for **2** in $CHCl_3$.

The electrochemical property of **5** was investigated using cyclic (CV) and square-wave (SWV) voltammetries in chloroform containing 0.1 M $TBAPF_6$ as a supporting electrolyte and in solid state containing HCl as a supporting electrolyte (Fig. 12, Table 4, S1 and S2). All the measured redox potentials, HOMO/LUMO and band gap energy E_g values obtained from those are tabulated in Table 4. As shown in Figs. 12 and 13, compound **5** displays reduction processes in their cyclic and square-wave voltammetries. Cyclic voltammogram of compound **5** has shown two fast reversible, one-electron reductions at −0.827 and −1.018 V (vs. $Ag/AgNO_3$, scan rate: 100 mV s^{-1}) with peak potential separations $\Delta E_{p1} = 76$ mV and $\Delta E_{p2} = 72$ mV, respectively in $CHCl_3$ (Fig. 12(a), Table 4). For compound **5**, the calculated ΔE_p in the range of 60–70 mV shows that reversibility of electron transfer was fairly well maintained in this system. The square-wave voltammograms of **5** (Fig. 12(b)) showed reversible reduction potentials at −0.830 and −1.026 V (vs. $Ag/AgNO_3$, frequency: 60 Hz). Similar results were found via cyclic and square-wave voltammetric studies. These properties are in agreement with the literature data [11].

In order to investigate the solid state electrochemical properties of compound **5** the voltammetry of immobilized microparticles was

Table 4
Cyclic[a] voltammetry data and optical band gap energy E_g, HOMO, LUMO values of compounds **1**, **2** and **5**.

	E_{pc}/V	E_{pa}/V	ΔE_p/mV	$E_{1/2}$/V vs. $Ag/AgNO_3$	E_{Fc}/V vs. $Ag/AgNO_3$	$E_{1/2}$/V vs. Fc	E_g/eV	HOMO/eV	LUMO/eV
1[b] (DCM)	−0.729	−0.662	67	−0.695	0.172	−0.867	3.21	−7.14	−3.93
	−1.157	−1.097	60	−1.127	0.172	−1.299			
2[b] ($CHCl_3$)	−0.825	−0.728	97	−0.776	0.234	−1.010	3.15	−6.94	−3.79
	−1.226	−1.127	99	−1.176	0.234	−1.411			
5[b] ($CHCl_3$)	−0.865	−0.789	76	−0.827	0.196	−1.023	2.28	−6.06	−3.78
	−1.054	−0.982	72	−1.018	0.196	−1.214			
5[c] (solid state)	−0.244	−0.378	134	−0.311[d]	0.360[d]	−0.671	1.92	−6.05	−4.13

[a] Scan rate of 100 mV s^{-1}.
[b] Supporting electrolyte: 0.1 M tetrabutylammonium hexafluorophosphate ($TBAPF_6$).
[c] Supporting electrolyte: 1 M HCl.
[d] vs. Ag/AgCl.

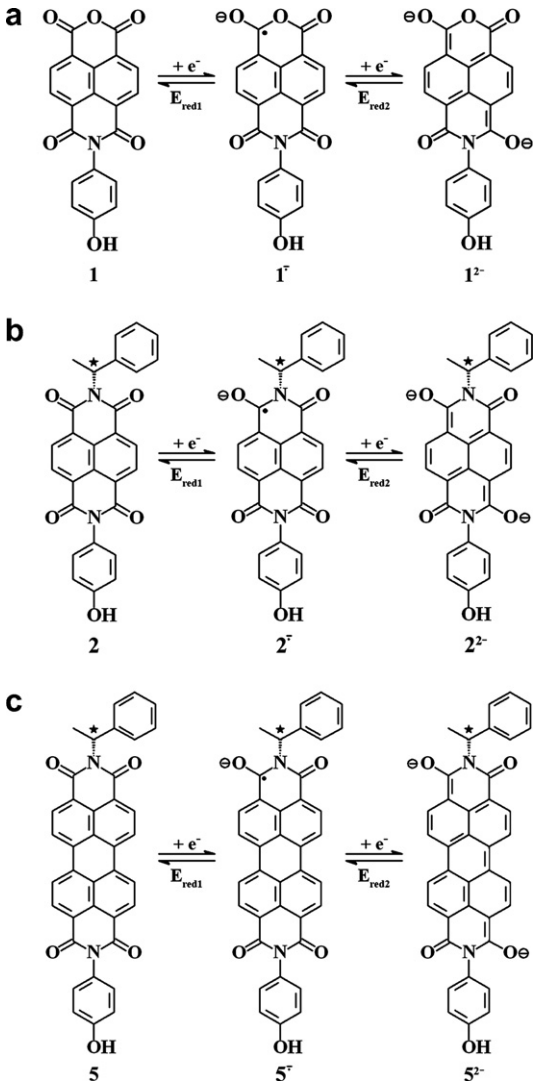

Fig. 13. Proposed two-step reduction mechanism for (a) **1**; (b) **2**; and (c) **5**.

applied. This technique is a simple and powerful tool for characterizing the thermodynamics and elucidating the redox mechanisms of electroactive compounds which are poorly soluble in water [49–56]. The basic principle of the voltammetry of immobilized microparticles comprises mechanical attachment of the substance on the surface of the working electrode (paraffin impregnated graphite electrode, i.e., PIGE), and immersing the modified electrode in an aqueous electrolyte solution. If the substance is electroactive, and if its product is also insoluble in water, for reasons of charge neutrality, ions must be exchanged with the solution. In case of a reduction, either anions, if available, must leave the solid, or cations must be transferred from the solution into the solid phase. The processes of coupled electron and ion transfer occur simultaneously and give rise to a single voltammetric response. A comprehensive database of the voltammetry on immobilized microparticles can be found elsewhere [56]. All the voltammetric measurements were repeated several times and the values of the reduction potentials were found to be reproducible within ±3 mV.

The solid state electrochemical property of **5** was determined with cyclic (CV) and square-wave voltammetries (CV and SWV: Fig. 12(c), (d) and Table 4, S2). All the measured redox potentials, band gap energies and the HOMO/LUMO values obtained from those are tabulated in Table 4. The cyclic voltammograms of compound **5** showed one reversible reduction waves (Fig. 12(c)), implying the formation of anions ($\mathbf{5}^{-}$) at −0.311 V (vs. Ag/$AgNO_3$, scan rate: 100 mV s^{-1}) with a peak potential separation ΔE_{p1} = 134 mV (Table 4). Similarly, the square-wave voltammograms of **5** (Fig. 12(d)) showed reversible reduction potential at −0.325 V (vs. Ag/$AgNO_3$, frequency: 50 Hz). Cyclic and square-wave voltammetric results were in good agreement. The reduction potential value is more positive than that observed for free **5** in solution indicating the easier reduction with higher reduction rate (Table 4). The compound **5** has shown lower solid state reduction potentials compared to the reductions of CN-substituted naphthalene and perylene derivatives [4]. On the other hand, the symmetrically substituted chiral perylene diimide bearing the same chiral substituent with compound **5** has the same solid state reduction potentials with it [21]. All solid state reduction potentials were measured with similar way. This interesting difference in results could be attributed to the intermolecular forces, rigidity and symmetry of the structure.

The electrochemical stability and reversibility of the redox processes of **5** was examined using cyclic voltammetry and square-wave voltammetries in $CHCl_3$ and solid state (Fig. 12(a–d), Tables S1 and S2). Electrochemical stability in $CHCl_3$ was examined by measuring repeated cycles of redox processes. **5** showed completely reversible reduction steps for the entire scanning rate in a region of 50–1000 mV s^{-1}. As shown in Table S1, the calculated peak current ratio, i_{pa} (anodic current)/i_{pc} (cathodic current) was equal to unity and the ΔE_p was about 70–103 mV for each cycle in $CHCl_3$. Notably, higher ΔE_p value (103 mV) at 1000 mV s^{-1}scanning rate shows more difficult reduction. According to standard reversibility criteria, each reduction process indicates reversible, diffusion-controlled one-electron transfer. Similarly, the solid state electrochemical stability and reversibility of the redox processes of **5** was examined using cyclic and square-wave voltammetries (Fig. 12(c) and (d), Table S2). Electrochemical stability of **5** was examined by measuring repeated cycles of redox processes. Compound **5** showed completely reversible reduction steps for the entire scanning rate in a region of 25–600 mV s^{-1} and 50–300 Hz. All voltammograms have shown only a slight shift of peak (SWV) or formal potentials (CV) of all compounds by 10 mV which indicate the electrochemical reversibility of the investigated system. As shown in Table S2, the calculated peak current ratio, i_{pa}/i_{pc} was equal to unity and the ΔE_p was about 134–164 mV for each cycle.

A plot of peak current against square root of scan rate was found to be linear as shown in Fig. S4 for compound **5** (in $CHCl_3$ $R^2 = 0.99$, in solid state $R^2 = 0.96$), which fulfills the conditions for diffusion-controlled processes. Additionally, at the large ΔE_p values which indicate the limitation due to charge transfer kinetics the reversibility of the compound showed poor reversibility.

The LUMO energies of **5** in $CHCl_3$ and solid state were calculated from cyclic voltammograms (Fig. 12(c) and (d), Table 4) as −3.78 and −4.13 eV, respectively. The optical band gap, E_g values, were calculated approximately 2.28 and 1.92 eV for the compounds, respectively where E_g was obtained from the edge of the solid state electronic absorption band. From these values, the HOMO energies of **5** were estimated as −6.06 and −6.05 eV, respectively. Remarkably smaller LUMO and E_g value were obtained at the solid state characterization of **5** as compared to those obtained from its solution state (Fig. 14). The diffusion coefficients D of **5** in $CHCl_3$ and solid state were measured by cyclic voltammetry according to Randles–Sevcik equation [48]. Accordingly, the diffusion coefficients were determined as 1.21×10^{-5} and 1.62×10^{-6} cm^2 s^{-1} for **5** in $CHCl_3$ and solid state, respectively.

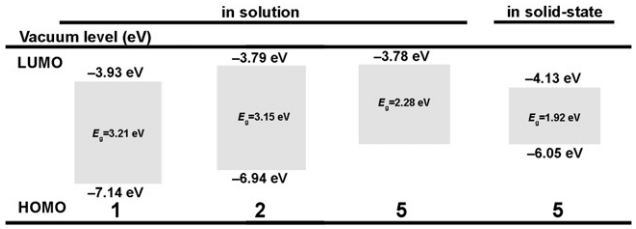

Fig. 14. Schematic energy diagram of **1**, **2** and **5**.

4. Conclusions

In conclusion, one new naphthalene monoimide (**1**) and two unsymmetrically substituted chiral diimides (**2** and **5**) having large π-conjugated systems have been successfully synthesized. At the same time, the perylene monoimide with the same substituent in naphthalene monoimide (**4**) has been synthesized according to the methods given in our previous works. Their structures have been well characterized and the photophysical, thermal, electrochemical, chiroptical and intramolecular charge transfer properties have been investigated. Imides **1**, **2** and **5** showed high thermal stability. Compound **1** exhibits an intramolecular charge transfer complexation in its absorption spectrum in polar solvent corresponding to a shift of the electron density from the electron rich moiety (hydroxyl substituent) towards the imide carbonyls. Additionally, the lower degree of symmetry of **1** may induce a higher number of vibronic modes which results in a broader absorption bands. The difference in complex formation between polar and non-polar solvents was attributed to the higher concentration of free reactive compound **1**. Excimer-like emissions were obtained in non-polar, polar protic and aprotic solvents for **1** and **2**. Interestingly, all the emission spectra of **1** and **2** show characteristically red shifted and broad excimer-like emissions. The large Stokes shifts and broadest band for the spectrum taken in NMP showed the presence of a relatively large amount of non-radiative energy lost. Moreover, it indicates that the configurations and interaction with the solvent of the excited and ground states are not similar. The fluorescence spectra of **4** and **5** showed mirror images of their absorption spectra with close and small Stokes shifts and absence of excimer emission in the same solvents used in the electronic spectra of **1** and **2** which proved the similarity between ground S_0 and excited S_1 states and high fluorescence quantum yield values. Solid state fluorescence of chiral compound **5** could not be obtained which is attributed to presence of excimers, which normally reduce quantum efficiencies of emission in the solid state. The electrochemical characteristics of compounds were investigated from dilute solution to solid state. In solution, compounds **1**, **2** and **5** showed two one-electron reductions. However in the solid state, chiral compound **5** has shown only one one-electron reduction which is consistent with the high molecular symmetry. Chiral **2** showed prominent negative Cotton effect centred at 362 and 382 nm however, **5** did not possibly due to the poor solubility comparing to the compound **2** at room temperature.

In summary, the results could lead to further development of sterically and stereochemically controlled conductive unsymmetrical diimides which could guide the design of important photo-, electro-, and optoelectronic devices.

Acknowledgments

The financial support from the Scientific and Technical Research Council of Turkey (TUBITAK) is gratefully acknowledged.

Appendix. Supplementary data

Supplementary data associated with this article can be found, in the online version, at doi:10.1016/j.dyepig.2009.04.014

References

[1] Todd EK, Wang S, Wan X, Wang ZY. Chiral imides as potential chiroptical switches: synthesis and optical properties. Tetrahedron Letters 2005;46:587–90.
[2] Zhou Y, Zhang D, Zhang Y, Tang Y, Zhu DJ. Tuning the CD spectrum and optical rotation value of a new binaphthalene molecule with two spiropyran units: mimicking the function of a molecular "AND" logic gate and a new chiral molecular switch. Journal of Organic Chemistry 2005;70:6164–70.
[3] Zhang J, Albelda MT, Liu Y, Canary JW. Chiral nanotechnology. Chirality 2005;17:404–20.
[4] Uzun D, Ozser ME, Yuney K, Icil H, Demuth MJ. Synthesis and photophysical properties of N, N′-bis(4-cyanophenyl)-3,4,9,10-perylenebis(dicarboximide) and N, N′-bis(4-cyanophenyl)-1,4,5,8-naphthalenediimide. Journal of Photochemistry and Photobiology A – Chemistry 2003;156:45–54.
[5] Dou Z, Li X, Zhong S, Zhao C, Na H. The synthesis and characterization of a novel ternary polymer bisphenol A-4,4′-difluorobenzophenone-bis(p-hydroxyphenyl)-1,4,5,8-naphthalenetetracarboxylic diimide monomer. Polymer Bulletin 2006;57:351–8.
[6] Figueiredo KM, Marcon RO, Campos IB, Nantes IL, Brochsztain S. Photoinduced electron transfer between cytochrome c and a novel 1,4,5,8-naphthalenetetracarboxylic diimide with amphiphilic character. Journal of Photochemistry and Photobiology B – Biology 2005;79:1–9.
[7] Nagao Y. Synthesis and properties of perylene pigments. Progress in Organic Coatings 1997;31:43–9.
[8] Shchepinov MS, Korshun VA, Egeland RD, Southern EM. Tritylisation of pyrene, perylene and coronene: a new family of switchable fluorescent labels. Tetrahedron Letters 2000;41:4943–8.
[9] Langhals H, Ismael R, Yürük O. Persistent fluorescence of perylene dyes by steric inhibition of aggregation. Tetrahedron 2000;56:5435–41.
[10] Tomizaki K, Loewe RS, Kirmaier C, Schwartz JK, Retsek JL, Bocian DF, et al. Of light-harvesting arrays comprised of a porphyrin bearing multiple perylenemonoimide accessory pigments. Journal of Organic Chemistry 2002;67:6519–34.
[11] Pasaogullari N, Icil H, Demuth M. Symmetrical and unsymmetrical perylene diimides: their synthesis, photophysical and electrochemical properties. Dyes and Pigments 2006;69:118–27.
[12] Baffreau J, Leroy-Lhez S, Anh NV, Williams RM, Hudhomme P. Fullerene c60-perylene-3,4:9,10-bis(dicarboximide) light-harvesting dyads: spacer-length and bay-substituent effects on intramolecular singlet and triplet energy transfer. Chemistry A European Journal 2008;14:4974–92.
[13] Hippius C, vanStokkum IHM, Gsänger M, Groeneveld MM, Williams RM, Würthner F. Sequential FRET processes in calix[4]arene-linked orange-red-green perylene bisimide dye zigzag arrays. Journal of Physical Chemistry C 2008;112:2476–86.
[14] Veldman D, Chopin SMA, Meskers SCJ, Groeneveld MM, Williams RM, Janssen RAJ. Triplet formation involving a polar transition state in a well-defined intramolecular perylenediimide dimeric aggregate. Journal of Physical Chemistry A 2008;112:5846–57.
[15] Gawroński J, Brzostowska M, Kacprzak K, Kołbon H, Skowronek P. Chirality of aromatic bis-imides from their circular dichroism spectra. Chirality 2000;12:263–8.
[16] Sterzel M, Pilch M, Pawlikowski MT, Gawroński J. The circular dichroism (CD) and absorption studies of 1,4,5,8-naphthalene tetracarboxydiimide dimer in terms of vibronic coupling theory. Chemical Physics 2003;291:251–60.
[17] Langhals H, Gold J. Chiral bifluorophoric perylene dyes with unusually high CD effects –- a simple model for the photosynthesis reaction center. Liebigs Annalen 1997;1997:1151–3.
[18] Langhals H, Krotz O. Chiral, bichromophoric silicones: ordering principles of structural units in complex molecules. Angewandte Chemie International Edition 2006;45:4444–7.
[19] Sun R, Xue C, Owak M, Peetz RM, Jin S. Facile synthesis of chiral unsymmetric perylene tetracarboxylic diimides involving α-amino acids. Tetrahedron Letters 2007;48:6696–9.
[20] Zheng J, Qiao W, Wan X, Ping Gao J, Wang ZY. Near-infrared electrochromic and chiroptical switching materials: design, synthesis, and characterization of chiral organogels containing stacked naphthalene diimide chromophores. Chemistry of Materials 2008;20:6163–8.
[21] Amiralaei S, Uzun D, İcil H. Chiral substituent containing perylene monoanhydride monoimide and its highly soluble symmetrical diimide: synthesis, photophysics and electrochemistry from dilute solution to solid state. Photochemical and Photobiological Sciences 2008;7:936–47.
[22] Osswald P, Reichert M, Bringmann G, Würthner F. Perylene bisimide atropisomers: synthesis, resolution, and stereochemical assignment. Journal of Organic Chemistry 2007;72:3403–11.
[23] Xue C, Chen M, Jin S. Synthesis and characterization of the first soluble non-racemic chiral main-chain perylene tetracarboxylic diimide polymers. Polymer 2008;49:5314–21.

[24] Dehm V, Chen Z, Baumeister U, Prins P, Siebbeles LDA, Würthner F. Helical growth of semiconducting columnar dye assemblies based on chiral perylene bisimides. Organic Letters 2007;9:1085–8.
[25] Tröster H. Untersuchungen zur Protonierung von Perylen-3,4,9,10-tetracarbonsäurealkalisalzen. Dyes and Pigments 1983;4:171–7.
[26] Hopkins HP, Stevenson KA, Wilson WD. Enthalpy and entropy changes for the intercalation of small molecules to DNA.I. Substituted naphthalene monoimides and naphthalene diimides. Journal of Solution Chemistry 1986; 15:563–79.
[27] Lokey RS, Kwok Y, Guelev V, Pursell CJ, Hurley LH, Iverson BL. A new class of polyintercalating molecules. Journal of the American Chemical Society 1997;119:7202–10.
[28] Gianolio DA, Segismundo JM, McLaughlin LW. Tethered naphthalene diimide-based intercalators for DNA triplex stabilization. Nucleic Acids Research 2000;28:2128–34.
[29] Asseline U, Cheng E. Synthesis and binding properties of perylene-oligo-2′-deoxyribonucleotide conjugates. Tetrahedron Letters 2001;42:9005–10.
[30] Rahe N, Rinn C, Carell T. Development of donor-acceptor modified DNA hairpins for the investigation of charge hopping kinetics in DNA. Chemical Communications 2003;17:2120–1.
[31] Lewis FD, Zhang L, Kelley RF, McCamant D, Wasielewski MR. A perylenedicarboxamide linker for DNA hairpins. Tetrahedron 2007;63:3457–64.
[32] Haga M, Ohta M, Machida H, Chikira M, Tonegawa N. Point-to-point capture of DNA with the aid of intercalation by immobilized rod-shaped Ru complexes at solid surface towards nanowiring. Thin Solid Films 2006;499:201–6.
[33] Zandonella G, Haalck L, Spener F, Faber K, Paltauf F, Hermetter A. Enantiomeric perylene-glycerolipids as fluorogenic substrates for a dual wavelength assay of lipase activity and stereoselectivity. Chirality 1996;8:481–9.
[34] Horne WS, Ashkenasy N, Ghadiri MR. Modulating charge transfer through cyclic D, L α-peptide self-assembly. Chemistry 2005;11:1137–44.
[35] Ashkenasy N, Horne WS, Ghadiri MR. Design of self-assembling peptide nanotubes with delocalized electronic states. Small 2006;2:99–102.
[36] Thalacker C, Würthner F. Chiral perylene bisimide-melamine assemblies: hydrogen bond-directed growth of helically stacked dyes with chiroptical properties. Advanced Functional Materials 2002;12:209–18.
[37] Schenning APHJ, Herrikhuyzen Jv, Jonkheijm P, Chen Z, Würthner F, Meijer EW. Photoinduced electron transfer in hydrogen-bonded oligo(p-phenylene vinylene)–perylene bisimide chiral assemblies. Journal of the American Chemical Society 2002;124:10252–3.
[38] Herrikhuyzen Jv, Syamakumari A, Schenning APHJ, Meijer EW. Synthesis of n-type perylene bisimide derivatives and their orthogonal self-assembly with p-type oligo(p-phenylene vinylene)s. Journal of the American Chemical Society 2004;126:10021–7.
[39] Würthner F, Chen Z, Hoeben FJM, Osswald P, You CC, Jonkheijm P, et al. Schoot PPAMvd, Meijer EW, Beckers EHA, Meskers SCJ, Janssen RAJ. Supramolecular p–n-heterojunctions by co-self-organization of oligo(p-phenylene vinylene) and perylene bisimide dyes. Journal of the American Chemical Society 2004;126:10611–8.
[40] Masu H, Mizutani I, Kato T, Azumaya I, Yamaguchi K, Kishikawa K, et al. Foldamers with iminodicarbonyl linkers: their stabilities and application to a chiral photochromic system using retro [4 + 4] cycloaddition. Journal of Organic Chemistry 2006;71:8037–44.
[41] Franke D, Vos M, Antonietti M, Sommerdijk NAJM, Faul CFJ. Induced supramolecular chirality in nanostructured materials: ionic self-assembly of perylene-chiral surfactant complexes. Chemistry of Materials 2006;18: 1839–47.
[42] Lukas AS, Miller SE, Wasielewski MR. Femtosecond optical switching of electron transport direction in branched donor–acceptor arrays. Journal of Physical Chemistry B 2000;104:931–40.
[43] Andric G, Boas JF, Bond AM, Fallon GD, Ghiggino KP, Hogan CF, et al. Spectroscopy of naphthalene diimides and their anion radicals. Australian Journal of Chemistry 2004;57:1011–9.
[44] Wilson JN, Gao J, Kool ET. Oligodeoxyfluorosides: strong sequence dependence of fluorescence emission. Tetrahedron 2007;63:3427–33.
[45] Turro NJ. Molecular photochemistry. New York, W.A.: Benjamin, Inc; 1965. 4–48.
[46] Peng Z, Bao Z, Galvin ME. Polymers with bipolar carrier transport abilities for light emitting diodes. Chemistry of Materials 1998;10:2086–90.
[47] Bredas JL, Silbey R, Boudreaux DS, Chance RR. Chain-length dependence of electronic and electrochemical properties of conjugated systems: polyacetylene, polyphenylene, polythiophene, and polypyrrole. Journal of the American Chemical Society 1983;105:6555–9.
[48] Bard AJ, Faulkner LR. Electrochemical methods, fundamentals and applications. New York: Wiley & Sons Inc; 1980.
[49] Kahlert H, Retter U, Lohse H, Siegler K, Scholz F. On the determination of the diffusion coefficients of electrons and of potassium ions in copper(II) hexacyanoferrate(II) composite electrodes. Journal of Physical Chemistry B 1998;102:8757–65.
[50] Lovric M, Scholz F. A model for the coupled transport of ions and electrons in redox conductive microcrystals. Journal of Solid State Electrochemistry 1999; 3:172–5.
[51] Lovric M, Hermes M, Scholz F. Solid state electrochemical reactions in systems with miscibility gaps. Journal of Solid State Electrochemistry 2000;4:394–401.
[52] Schröder U, Scholz F. The solid-state electrochemistry of metal octacyanomolybdates, octacyanotungstates, and hexacyanoferrates explained on the basis of dissolution and reprecipitation reactions, lattice structures, and crystallinities. Inorganic Chemistry 2000;39:1006–15.
[53] Hermes M, Lovric M, Hartl M, Retter U, Scholz F. On the electrochemically driven formation of bilayered systems of solid Prussian-blue-type metal hexacyanoferrates: a model for Prussian blue/cadmium hexacyanoferrate supported by finite difference simulations. Journal of Electroanalytical Chemistry 2001;501:193–204.
[54] Widmann A, Kahlert H, Petrovic-Prelevic I, Wulff H, Yakhmi JV, Bagkar N, et al. Structure, insertion electrochemistry and magnetic properties of a new type of substitutional solid solutions of copper, nickel and iron hexacyanoferrates/hexacyanocobaltates. Inorganic Chemistry 2002;41:5706–15.
[55] Grygar T, Marken F, Schröder U, Scholz F. Electrochemical analysis of solids. Collection of Czechoslovak Chemical Communications 2002;67:163–208.
[56] Entire database of bibliography on the voltammetry of immobilized microparticles is available on: http://www.chemie.uni-greifswald.de/~analytik/